4 High Repetition Rate X-Ray Generation Using Liquid Jet Targets

One of the main goals of this work is the construction and evaluation of a high-repetition rate source for hard X-ray pulses. Following the description of the laser system and the target setup presented in the previous chapters, this chapter details first results of the X-ray generation experiments. The observed spectra include line radiation as well as continuous bremsstrahlung. For the spectral characterization of the emitted X-rays, a dispersive silicon detector was employed. This chapter begins with a description of the detection system including a detailed discussion of its benefits and limitations. Subsequently, the investigations of X-ray emission from gallium jet targets are presented. These include measurements of output characteristics such as photon number, and also more technical details like long-term stability and debris emission. While the principal interest applies to the gallium jet X-ray source, the production of broad-band X-rays with water and gold targets will be presented too. Although physically and chemically rather different, gallium and water have both specific advantages as target material for X-ray generation. This chapter will close with a discussion of the advantages and disadvantages of these materials for the generation of hard X-rays.

4.1 Spectral Measurements of Hard X-Rays Using a Dispersive Silicon Detector

X-ray spectra have been recorded for almost one century. In most cases, crystals or gratings have been used to disperse the radiation. Instruments using these principles are reliable and offer high precision. Recent progress in solid-state physics and electronics allows for the development of new systems relying on photon absorption in semiconductors. All of the experiments presented in this work utilize a dispersive silicon detector (XR100-CR, AMPTEK, Inc.). The basic principle of its operation is described below:

Essentially, the detector consists of a 300 μm thick silicon chip. Incoming X-ray photons interact with silicon atoms by creating an average of one electron/hole pair for every 3.62 eV of photon energy absorbed in the silicon. Depending on the X-ray energy, the loss mechanism

is dominated either by the photoelectric effect or (at higher energies) by Compton scattering. The charges created are collected in the chip and the resulting signal is amplified. The amplitude of the resultant signal is proportional to the energy of the absorbed X-ray photon. A multi-channel analyzer (MCA) was used for acquisition and analysis of the detector output. The MCA arranges the data in a histogram and makes it available for transmission to a personal computer every 7 sec. Appropriate computer software allows long time-data collection, spectral calibration and data evaluation. As a consequence of its principle of operation, the silicon detector works only in the single-photon regime: if more than one photon arrives at the detector during the read-out time, the signal corresponds approximately to the sum of photon energies and exceeds the limit of the histogram acquired. Such signals are called 'pile up' and are found on the end of the MCA data set (=last effective channel). In order to achieve precise experimental results, the 'pile up' must be kept as low as possible. This can be accomplished a) by a larger distance to the X-ray source (unless it is a collimated beam), b) by use of an aperture on the detector which reduces the effective detector size, c) by an appropriate filter. Alternatively, an electronic pile-up rejection may be employed.

Filtering is necessary, anyway, in order to block low energy photons (IR photons from the laser and visible light from the plasma spark, in particular). This is accomplished by a beryllium window fixed on the silicon detector. Fig. 4-1 shows the transmission of different Be windows for soft X-rays. The Be-window defines the lower spectral limit of detection, while the upper limit depends on the decreasing efficiency of photon absorption (and Compton scattering) with higher photon energy. Fig. 4-2 shows the detection efficiency for

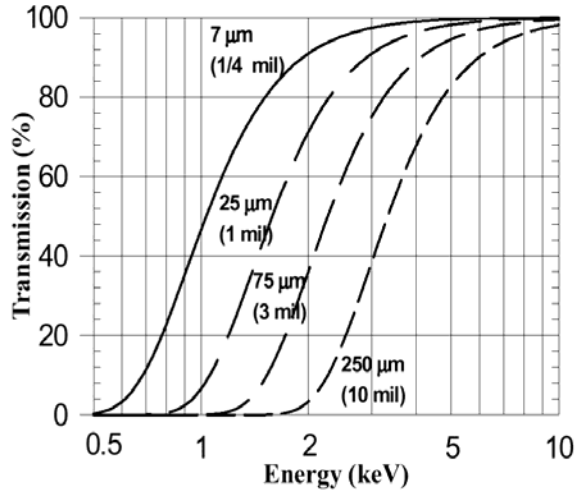

Fig. 4-1: Transmission of beryllium windows for soft X-rays depending on Be thickness [AMP].

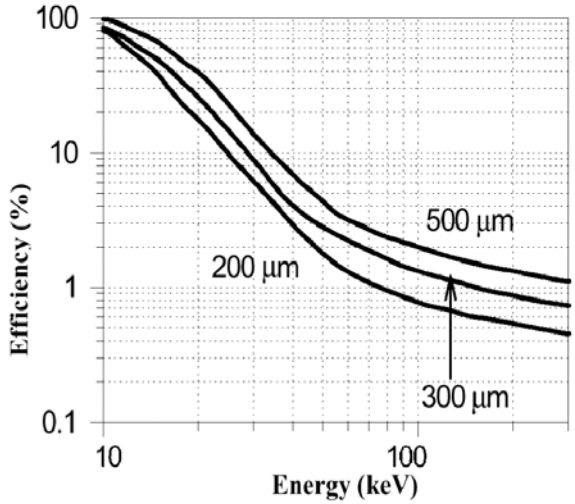

Fig. 4-2: XR100-CR detection efficiency for hard X-rays depending on silicon thickness [AMP].

different thicknesses of the silicon chip of the detector itself. Our detector has a 25 µm Be-coating and a 300 µm thick silicon chip. From Fig. 4-1 and Fig. 4-2 it is apparent that the detector has optimum efficiency between about 5 and 10 keV. For the gallium line radiation at 9.2 keV and 10.3 keV, this is sufficient. Lower photon energies were not within the scope of our experiments. However, whenever photons of higher energies are analyzed, a correction function is necessary. Such a correction function (Fig. 4-3) has been calculated from the efficiency data presented above (see Appendix A and [AMP]), whose precision is not specified. Apparently, any measured noise within the data sets will be magnified with the application of the correction factor, too. Magnified noise in high energy regions exceed the signal at lower energies. Hence, the application of the correction function is limited by high energy noise and the contrast of the investigated spectral feature. However, as shown later (Fig. 4-16), reasonable results can be derived even for photons of 50 keV, provided the noise is small enough. If better efficiency in the hard X-ray region is desired, another detector material, e.g., cadmium telluride, has to be considered. A survey of the commercially available systems shows that AMPTEK offers a CdTe detector with a detection efficiency of some 60% at 100 keV photon energy.

For the further data processing a calibration of the spectrometer is necessary. The basic spectroscopic data from the instrument are given as counts per MCA channel to the PC. The proprietary AMPTEK software allows 2 ways for calibration: Recognizable peaks in the

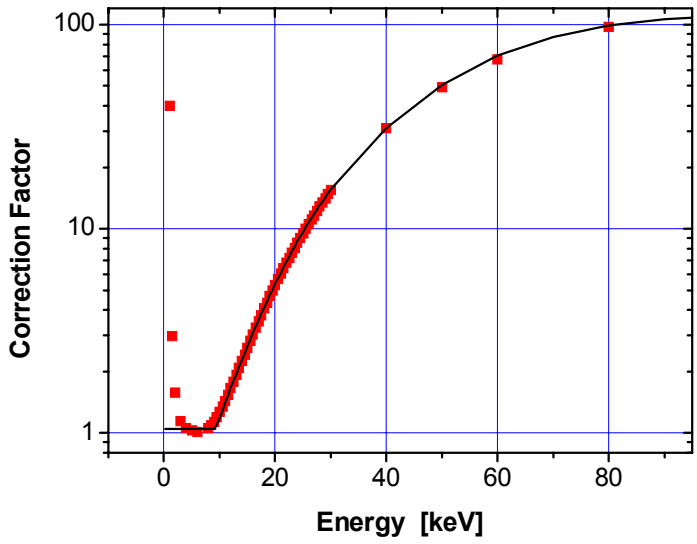

Fig. 4-3: Correction factor for hard X-ray spectra taken with XR100-CR spectrometer. The squares denote the reciprocal of efficiency numbers as given in Appendix A and the line shows an appropriate fit (3-fold exponential) which is used for high energy data correction.

spectrum can be associated with appropriate photon energies or wavelengths. If two or more peaks are assigned, a second (third) order polynomial fit is implemented. The fit-coefficients define the calibration of this particular spectrum. Usually the third-order coefficient gives only a small correction. The calibration is valid for one particular gain setting. If the gain of the signal amplifier is increased, the MCA channel number for one spectral feature increases too and the spectrum is spread out. Alternatively, one can use the raw data from the instrument for calibration and do a similar fit procedure using any other data processing software (e.g. MicroCal ORIGIN).

The precision of such a calibration is limited by the line width (220 eV resolution specified by manufacturer [AMP]) and by the number of peaks included in the polynomial fit. Fig. 4-4 shows a calibration spectrum from a ^{241}Am radioactive emitter. It has been taken by Stiel and Vogt [VOG02] with the instrument used for the gallium experiments. The gain was set to 2.5. The broadband spectra of water and gold (see section 4.3) were taken with different gain settings and were calibrated by using the characteristic line radiation of different metals. The specified spectral resolution of the AMPTEK XR100-CR of 220 eV is a lower limit. In the experiments larger values (e.g. 300 eV in Fig. 4-4) are measured, which are also dependent on the photon energy. For spectral measurements with higher precision requirements this instrument is not useful. In section 5.2 a setup with an excellent spectral resolution of about 1 eV will be presented, obtained with a diffracting crystal and a CCD-camera. With that device the doublet structure of the K_α line due to spin orbit splitting (27 eV) can be clearly resolved.

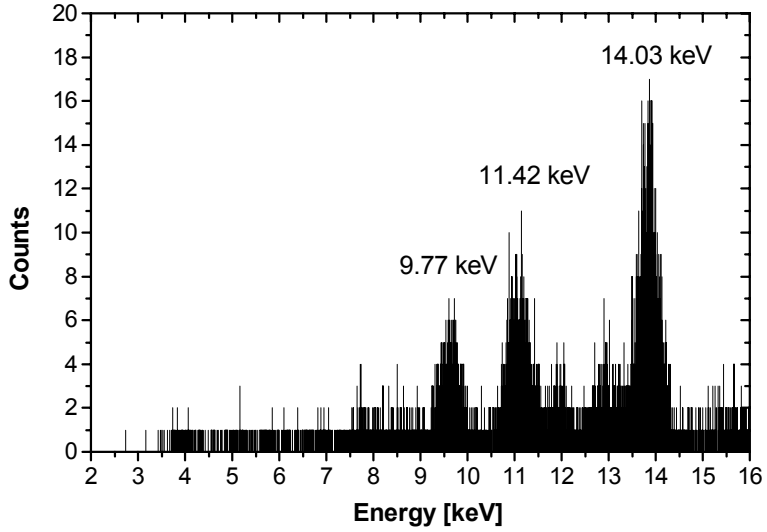

Fig. 4-4: ^{241}Am spectrum taken with XR100-CR (gain 2.5) for calibration [VOG02].

4.2 Generation of Gallium Line Radiation

Among the possible target candidates (see section 3.2) gallium has been chosen for the generation of hard X-rays. Its physical and chemical characteristics make it an outstanding candidate for this purpose. The intention was to develop a laser based source of hard X-ray line radiation with capability of high repetition rate. Gallium offered characteristic radiation at 9 and 10 keV, respectively. Its chemical properties guarantee easy handling at almost room temperature as well as low vapor pressure.

4.2.1 Experimental Setup

Fig. 4-5 shows a schematic of the experimental setup. The laser pulses are focused onto the gallium jet target using a plano-convex lens with 75 mm focal length and an open diameter of 20 mm (= laser beam diameter). The energetic radiation emanating from the target in the laser focus is measured with the dispersive silicon spectrometer in an appropriate distance. Depending on exposure this distance has to be varied between 750 mm and 1250 mm to obtain single-photon counting conditions. The Al-filter blocks low-energy radiation up to about 2 keV. The Pb aperture further reduces the exposure of the detector.

For investigations on the temporal stability of the X-rays several different diodes have been used. Most reliable among them is the AXUV–100 silicon diode (International Radiation

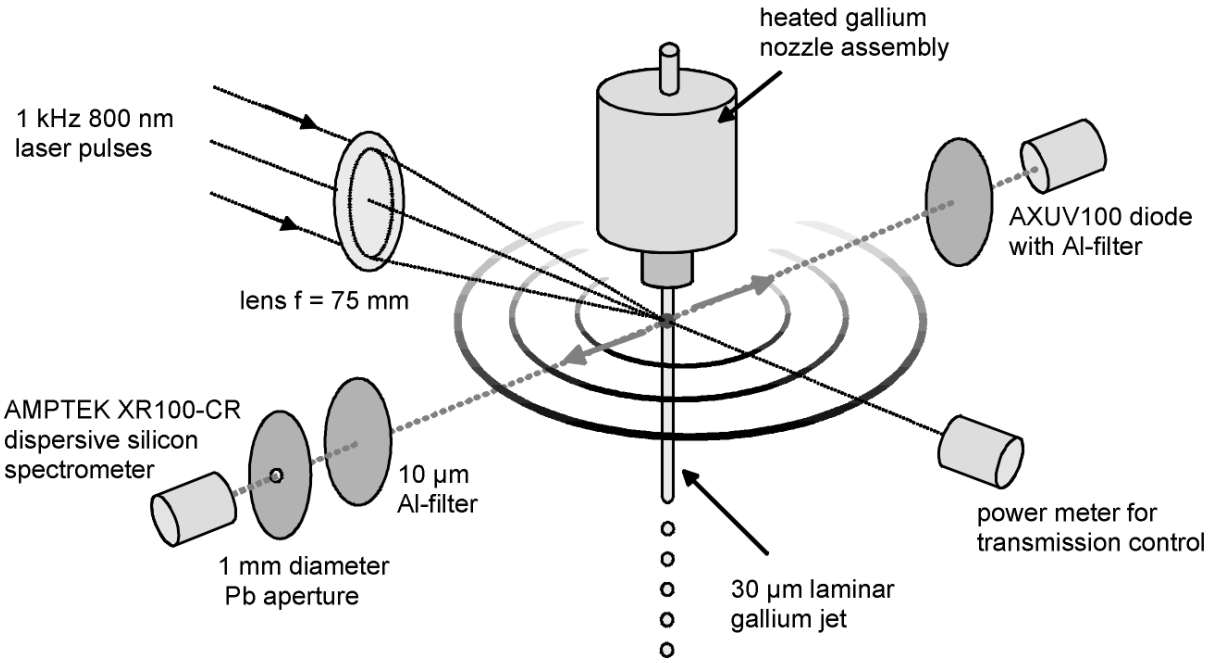

Fig. 4-5: Scheme of the experimental setup for X-ray measurements with gallium jet target.

Detectors, Inc.). These diodes are especially developed for x-ray measurements [IRD]. For improved noise reduction a pre-amplifier (AXUV-100HYB1/HYBV, IRD, Inc.) is mounted directly onto the diode. For the suppression of visible light and soft X-rays, the detector is coated with Cr/W/Au (80µm/1000µm/4000µm). This coating blocks all radiation with wavelengths $\lambda > 1$ nm ($E \leq 1$ keV). To block radiation with less than 4 keV photon energy, a 30 µm Al foil is added to the diode.

The jet itself is run in a vacuum chamber at about 0.1 mbar. To prevent absorption in air, the x-ray detectors are located in vacuum too. It should be noted that for x-ray experiments with more than 20 keV photon energies, vacuum conditions are not necessary for the X-ray transmission because T > 90% in nitrogen and oxygen (calculated for 1 m distance at 20 keV [LBL]). The gallium line radiation is absorbed a little but on short distances transmission in air should be possible. This can be helpful for alignment purposes of more sophisticated experiments. The laser based generation of X-rays itself must always be done in vacuum because at these high intensities the laser radiation would already be absorbed in air before the focal point.

A power meter is placed in line with the laser beam, far behind the laser focus, to measure the transmission of laser power through the plasma. This is an important indicator for the alignment of the jet-to-focus position. In principle, each effect which depends on optimum laser-plasma coupling can be used for alignment. Table 4-1 shows a choice of

Table 4-1: Optimization parameters for X-ray generation.

Indicator	**Limitation**
spectral X-ray yield of dispersive silicon spectrometer	needs about 7 s for one histogram read-out
integrated signal on the diode	>20% noise, integrates line and bremsstrahlung
hard x-ray emission outside the chamber measured with doserate meter TOL/F (for more details see section 4.3.2)	too small amplitude in gallium experiments, only up to 10 µSv/h, read-out time about 5 s
backscattered radiation (e.g. blue SHG from critical surface)	not reliable for yield optimization but valuable for lateral overlap alignment
laser power transmission	instantaneous parameter for lateral and longitudinal focus-to-jet overlap

Five indicators that were investigated for optimization of X-ray yield. In the gallium experiments laser transmission has proven to be the best. The indication is instantaneous and the precision is limited in lateral direction only by the translation stage of the jet (< 5 μm). In line with the laser the necessary alignment precision is less critical because the Rayleigh length of the laser focus is larger than the jet diameter. In this case the precision of the translation stage for the jet movement (laser focus position was fixed by the lens) was fully sufficient with 5 μm precision. The coincidence of lowest laser transmission and highest conversion efficiency into X-rays has been proven using the AMPTEK spectrometer. For practical reasons the transmitted laser light is measured outside the vacuum chamber and directed onto the power meter with a large aperture lens.

An alignment along the z-axis (= jet-axis) has no influence on the conversion efficiency provided the laser hits the laminar part of the jet and is not blocked by parts of the nozzle accessories.

4.2.2 Generation of Gallium Line Radiation at kHz Repetition Rate

The first gallium X-ray spectrum (Fig. 4-6) achieved with the above described apparatus, includes K_α and K_β characteristic line radiation as well as broadband continuum between 5 and 15 keV. In this section the experimental results will be discussed regarding line radiation while broadband features will be discussed in more detail in section 4.3.

Because of the single-photon counting principle, the spectrometer counts of Fig. 4-6 (ordinate) directly correspond to the number of photons. Flux numbers are derived as follows: The count rate of detected photons N_{det} is calculated from the number of detected counts Z_{cts}

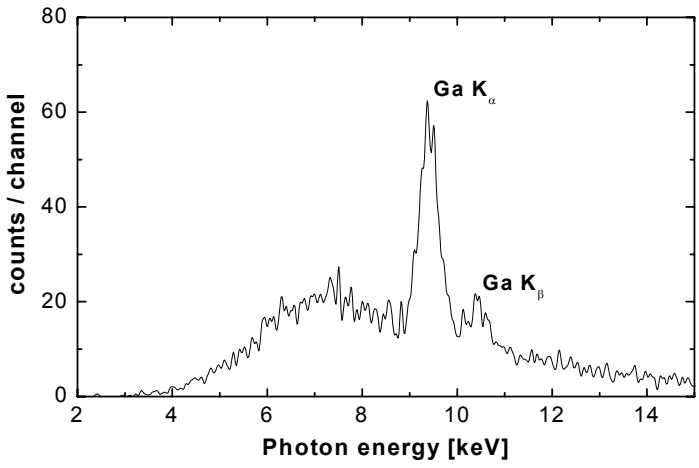

Fig. 4-6: First gallium X-ray spectrum.

and the live time of the detector T : $N_{det}=Z_{cts}/T$. Assuming isotropic emission, the emission rate N_{em} (emitted photons per second) is given by $N_{em}=N_{det}*4l^2/\pi d^2$, where l is the distance from the source to the detector and d is the diameter of the detector aperture. The emitted flux Φ into a spatial angle of 1 sr is calculated as $\Phi=N_{em}/4\pi$.

In a first experiment (Fig. 4-6) with the detector (aperture d=2 mm) at l = 300 mm distance from the source an average of N_{det}=19 photons/s was detected. Integration over about 1 keV line width at 9.3 keV gives a rate of 4.4 photons/s for the K_α line radiation. This corresponds to an emission rate of of 1.6×10^6 s^{-1} assuming isotropic emission. The total emission rate with E < 16keV is $6.8\times10^6 s^{-1}$. The laser parameter were: pulse length 50 fs, pulse energy 2 mJ 1 kHz repetition rate and an intensity of 3×10^{16}W/cm² (assuming gaussian profile and 86% energy confinement, see section 3.1.2).

With an improved alignment procedure (see previous section) it was possible to increase the coupling efficiency of the laser and to shift the broadband radiation to higher energies. An example of such a measurement is presented in Fig. 4-7. The units for the photon flux in this graph are chosen as photons/(s*sr*keV). This takes into account that the amplitude in a simple spectrum like Fig. 4-6 shows only the number of collected counts per spectrometer channel. If the spectral width of such a channel is changed (e.g. by changing gain and calibration) then the same peak would have a different amplitude because the same number of photon events would be sorted into a different number of channels. Therefore it makes sense to divide the actual count number in each channel by its spectral width (= 16 eV in the applied calibration) and to select photons/(s*sr*keV) as unit of the spectral amplitude. For the determination of total numbers of line radiation, the peak values from the spectrum would not be sufficient. Because of the finite width of the line radiation peak[1] due to the instrument uncertainty, it is necessary to sum up all counts belonging to the peak. In this case the numbers are independent of the scaling and the unit 1/(s*sr) or 1/(s*4π sr) ≡ 1/s, respectively, can be used again.

The spectrum Fig. 4-7 was measured with similar laser parameters as described above. Improved laser-to-X-ray efficiency allowed detection at a longer distance (l=700mm) with a smaller aperture (d=1mm). In the spectrum the broadband peak is not visible. The small peaks at 8 keV and 6.4 keV are due to line radiation from Cu and Fe parts, respectively. This radiation emanates probably from copper and iron in the nozzle apparatus itself and from a copper hose holder attached to the nozzle. The small rise on the upper end of the spectrum is due to higher hot electron energy and therefore to an up-shifted broadband bremsstrahlung

[1] The natural line width is in the order of 2.6 eV . [KO79]

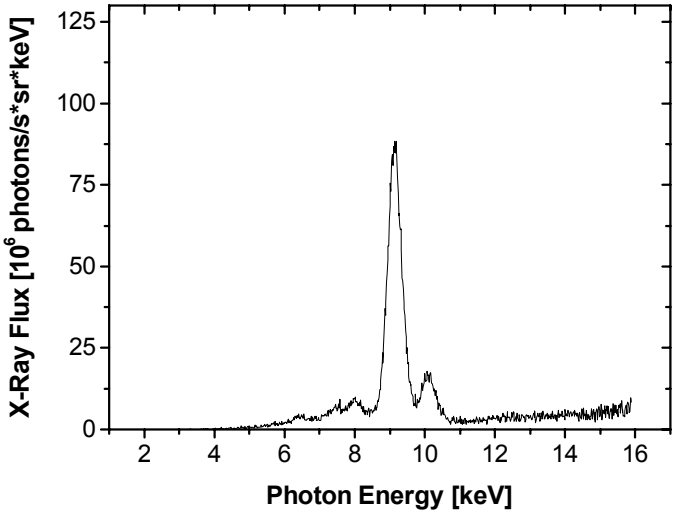

Fig. 4-7: Gallium X-ray spectrum obtained with improved alignment.

spectrum (for comparison see Fig. 4-16 a). The emission rates are improved: the K_α line has 5.5×10^8 photons /s assuming a line width of 1 keV (due to spectrometer resolution) and the total number of photons with $E < 16$ keV is increased to 11.4×10^8 photons/s. The relation between line and total radiation is about 1:2 (pile up excluded). Typical recording time for such a spectrum is about 200 s. The total energy per second in the line radiation was calculated to 0.8 μJ. This corresponds to an laser-to-X-ray conversion efficiency of 4×10^{-5} %.

In Table 4-2 the flux data from the experiments presented here are compared with other published results. Before discussing these numbers, a few remarks should be made:

a) up to a about 10^{17} … 10^{18} W/cm² the conversion efficiency increases with the applied laser intensity (see e.g. RGU00). So, the 10…20 Hz laser systems with inherently higher pulse energies should have higher conversion efficiencies due to their higher intensities.
b) Laser intensities are not given in all publications and if so only a few researcher mention how they define their intensity in the focus. Therefore this is a vague criterion for comparison.
c) Fortunately, many groups used similar detectors from AMPTEK, Inc. These are directly comparable with the numbers presented above. The data of Jiang et al. [JRP02] and Eder et al. [MPQ00] were recorded with CCD Cameras. This method depends on image-processing software and the spectral resolution there is different from the AMPTEK device. Most precise data is probably coming from Feurer et al. [FEU01], where an absolutely calibrated Pentaerytrit (PET) von-Hamos spectrometer was used.

d) As unit for the flux, "photons per second and per 4π steradians" is chosen in most of the publications concerning laser produced plasma. It is equal to the emission rate in photons per second and it should be clearly distinguished from "photons/(s*sr*keV)" as used in the figures above. Some numbers in Table 4-2 have been calculated from published data assuming isotropic X-rays emission.

e) Laser systems here are all titanium:sapphire systems. Therefore their emission wavelength is always about 800 nm. The pulse structure and length is different in the experiments, some groups use pre-pulses (e.g. [RRU97]).

It is remarkable that among the kHz systems, the results of the gallium experiments exhibit the highest laser-to-K_α efficiency ($\varepsilon = 4.1 \times 10^{-7}$). Results from the Rose-Petruck group [JRP02] show a similar X-ray emission rate while using shorter pulses (higher pulse power) and double the repetition rate, so the efficiency is lower: $\varepsilon = 1.6 \times 10^{-7}$.

Table 4-2: Emission rate of X-ray line radiation and efficiency of different sources.

Reference	Laser	Target	Line emission rate	Efficiency[1]
T. Guo et al. [GUO97]	20 Hz, 30 fs, 75 mJ	Cu wire	Cu K_α 8 keV 5×10^{10} s^{-1}	0.0043 %
Rischel / Rousse et al. [RRU97], [RRF01]	10 Hz, 130 fs, 15 mJ	silicon plate	Si K_α 1.7 keV (≡7.1 Å) 8.5×10^{8} s^{-1}	1.5×10^{-4} %
Feurer et al. [FEU01]	10 Hz, 80 fs, 0.2 J 5×10^{17} W/cm²	silicon	Si K_α 1.7 keV 6×10^{10} s^{-1}	8.2×10^{-4} %
Eder et al. [MPQ00]	10 Hz 200 fs, 0.2 J 10^{17} W/cm² (for highest K_α yield)	Cu plate	Cu K_α 8 keV 1×10^{12} s^{-1}	0.064 %
Tompkins et al. [TMF98]	1 kHz, 100 fs, 0.5 mJ appr. 10^{16} W/cm²	200 µm water jet with solved $Cu(NO_3)_2$	5…10 keV, peak at 9keV 10^{7} s^{-1}	2.9×10^{-6} %
Jiang et al. [JRP02]	2 kHz, 40 fs, 3.3 mJ	Cu wire	Cu K_α 8 keV 8×10^{8} s^{-1}	1.6×10^{-5} %
This work [KOR02]	1 kHz, 50 fs, 2 mJ 3×10^{16} W/cm²	gallium jet	Ga K_α 9.2 keV 5.5×10^{8} s^{-1}	4.1×10^{-5} %

[1] Efficiency calculated as (emitted X-ray line energy per second) / (deposited laser energy per second)

4.2.3 X-Ray Generation at 10 kHz Repetition Rate

To test the capability of the gallium system at even higher repetition rates, the laser system was modified. With a different amplifier setup, a repetition rate of 10 kHz has been achieved. For this purpose the post-amplifier was seeded directly from the oscillator and pumped by a 10-kHz green laser (CORONA, Coherent Inc.) with 70 W of green light at 532 nm. The output after recompression was 4.5 W (corresponding to 0.45 mJ per pulse). On the target location 2.2 W (= 0.22 mJ per pulse) of laser power were detected. The experimental setup was similar to Fig. 4-5. The pressure in the gallium reservoir was 50 bar and the nozzle diameter 30 µm. Outside the chamber a radiation dose rate of 25 µSv/h was measured (TOL/F, BERTHOLD Technologies) which is about 250 times the background level and similar to the numbers during 1-kHz experiments. Because of the low flux, the distance between the dispersive silicon spectrometer (AMPTEK XR100-CR) and the laser focus was set to a shorter distance d = 400 mm.

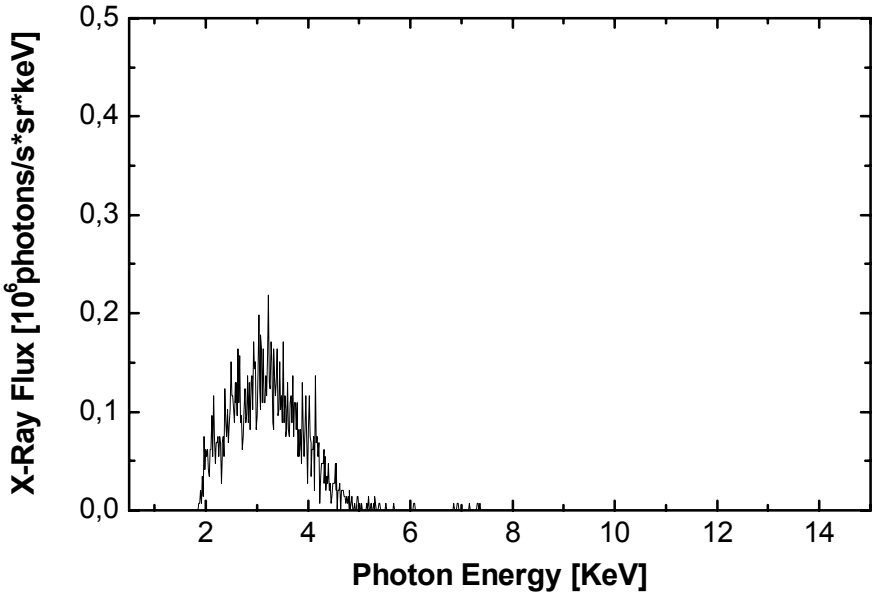

Fig. 4-8: Broadband spectrum from gallium target at 10 kHz laser repetition rate.

The spectrum of Fig. 4-1 shows a broad distribution around 3.5 keV. As mentioned earlier such a distribution is due to the bremsstrahlung of hot electrons decelerated in cold target material. One can conclude from this spectrum that the energy of these hot electrons was to small to remove inner shell electrons. Therefore no gallium line radiation could be created. To produce line radiation efficiently with this system the intensity has to be increased to transfer more energy to the hot electrons. Details of the transfer process itself will be discussed in the

next section. Some additional technical improvements to establish higher laser intensity and hence, higher conversion efficiency, should be mentioned here:

a) Decreasing the laser focus size. This can be done using optics with higher f-number (e.g. off-axis parabola mirror) or by using adaptive optics (e.g. for a 1 kHz system [ALB00])
b) Increasing the laser pulse energy. As has been shown in the 1 kHz experiments above, with similar optics a pulse energy of about 2…3 mJ is sufficient for the generation of Ga line radiation. But under the given conditions this would imply 10 times larger pump power for amplification at 10 kHz. Such pump lasers are currently not available.
c) Advanced pulse structuring. Shorter laser pulses (e.g. [GUO97]) lead to higher efficiency. Furthermore an increase of a factor of 7 was reported [RRU97] when using appropriate prepulses. Best results (factor 27 increase) were found with an adaptive optimization of energy and distance of the prepulse, relative to the main pulse by Feurer [TF99].

These are a few simple ways to improve the efficiency of the X-ray generation. In the next section a more sophisticated detailed of the energy transfer process and the optimization parameters will be given.

4.2.4 Discussion of the Energy Transfer Process and Optimal Parameters

The results shown in the figures above offer a good opportunity to review some theoretical background and to discuss the processes involved for the conversion of ultra-short laser pulses into X-ray line radiation. This is typically done in two steps: First we will focus on the absorption process of the laser light and the conversion into hot electrons. Then the energy transfer from hot electrons to x-ray photons will be considered.

Resonance absorption has been investigated already in the 1970s (e.g. [FOR77], [EST78]) with two dimensional particle-in-cell (PIC) codes in order to understand the transfer process from intensive laser pulses to hot electrons. Brunel [BRU87] added his idea of “vacuum heating” (electron heating in the vacuum outside the plasma) to explain the efficient absorption at higher intensities. In the 1990s the advent of sub-ps lasers required the anticipation of steeper density gradients in the plasma [GB92] and also of intensities greater than 10^{18} W/cm² [WKT92]. But the physics at these intensities is beyond the scope of this work. An overview of these investigations and their history is given in a number of review articles (e.g. [GIB96]).

All these simulations and early experiments found a similar dependence of the hot-electron energy T_{hot} (keV), on laser intensity I (usually in units of 10^{16} W/cm²) and the wavelength λ (μm):

$$T_{hot} \propto C * (I\lambda^2)^{\alpha} . \qquad / 4\text{-}1$$

C denotes a constant and in some calculations [FOR77] can contain the background electron temperature at the critical density. Experimentally as well as by fitting the results from simulation the exponent α was found to be between 0.25 and 0.5.

For an estimation of numbers applicable to the results in our work, two more recent papers will be used [RGU00], [SRU02]. In the first of these publications 1D oblique incidence particle-in-cell (PIC) simulations were performed to obtain hot electron distributions $f_{hot}(E)$. The initial conditions for the simulations were: 60 fs, Ti:Sa-laser, 45° incidence angle, 100 mJ *constant* energy. An exponential plasma density gradient with scale length $L = 0.3\ \lambda$ takes into account small pre-plasmas due to pre-pulses. The simulations were done for a variety of different laser intensities (varying focus diameter). Fitting these results led to a formula for the hot electron energy (temperature) similar to equation /4-1/ :

$$k_B T \approx 130keV * (I / 10^{17} Wcm^{-2})^{0.5} . \qquad / 4\text{-}2$$

For the laser intensity of 3×10^{16}W/cm² in our experiments, the formula gives a hot-electron temperature of 71 keV[1]. This corresponds to an electron velocity of 0.48c. The simulated energy distribution f_{hot} of the electrons was found to be fitted best by a one-dimensional Maxwellian distribution [RGU00]: $f(E)\,dE = (E\,k_BT)^{-0.5} \times exp(-E/k_BT)\,dE$.

For the optimization of a K_α line source, the conversion of hot electron energy into photons following the primary acceleration, is of particular interest. For the calculation of the number of X-ray photons N_{gen} generated out of one electron with the energy E, as a simple solution one could use a formula from the investigation of X-ray tubes (from [GCO68] slightly modified in [RGU00]):

$$N_{gen}(E) = 4\times10^{-3} Z^{-1.67} E^{3/2}, \qquad / 4\text{-}3$$

where Z is the atomic number of the target material. But this would neglect the non-trivial interplay of impinging electrons, the K-shell ionization energy of the target and the target thickness. At first the hot electrons have a certain stopping range (penetration depth) in the material depending on their energy and the atomic number of the material (following Reich et al. [RGU00] we neglect elastic scattering and spatial effects). The K-line photons generated

[1] In section 4.3 it will be shown that the estimated hot-electron temperature in the gallium experiments is about 55 keV.

by inelastic scattering of the electrons can be reabsorbed and , of cause, the probability of reabsorption increases with longer trajectories of the photons in the material. Therefore with increasing electron energy the penetration depth as well as the reabsorption increase. Because this scaling is inverse to the growth of photon yield with increasing electron energy one can expect a maximum of K_α photon generation depending on the incident electron energy. With the semi-empirical method this optimum was calculated (within the backscattering model as referred to above [RGU00]). The result implied an optimal laser intensity for a given material with atomic number Z:

$$I_{opt} = 7 \times 10^9 Z^{4.4}. \qquad / 4\text{-}4$$

This corresponds to an optimum hot electron temperature 6.4 times the K-shell ionization energy. For gallium this would lead to an optimum hot electron energy of about 60 keV. Using formula /4-4/ one can calculate optimum intensities for different target materials:

Table 4-3: Optimum Intensities for generation of line radiation (calculated using (7) from [RGU00]).

Target Material	Atomic number Z	K_α emission line [keV]	Optimum intensity I_{opt} [W/cm²]
Ti	22	4.5	6×10^{15}
Cu	29	8.0	2×10^{16}
Ag	47	22.1	1.6×10^{17}
Ta	73	57.5	1.1×10^{18}
Ga	31	9.3	2.5×10^{16}

Eder et al.[MPQ00] found experimental evidence for the existence of an optimum intensity as shown in Table 4-3. In their experiments, a decrease of intensity from 10^{18} W/cm² to about 10^{17} W/cm² gave an increase in Cu K_α yield by a factor of 2. This suggests that real optimum intensities might be slightly larger than the calculated numbers. For the measurement presented here, one can conclude that the parameters are within one order of magnitude around the optimum intensity value.

The simulations so far were done for bulk targets observing the (backscattered) K_α radiation normal to the targets surface. In the more recent work of the Jena group [SRU02], particular emphasis was put on the investigation of spatial dependencies. Fig. 4-9 shows the result of calculations with a more advanced model where the spatial dependence of the K_α generation and the reabsorption are taken into account explicitly without averaging over any emission region. In the graph the influence of target thickness (thin foils) on the photon emission is

shown for forward as well as for backward photons. This graph permits several interesting conclusions on the qualitative behavior of the emission process:

- Backward emission is always stronger than forward emission.
- There is always an optimal target thickness for forward emitted photons while the backward emission stabilizes on a level depending on the electron energy but not on target thickness.
- It exists an optimum electron temperature (and an optimum target thickness) for maximum emission of X-ray line photons.

Such conclusions can be very helpful for the engineering of new experiments: The first point, for instance, suggests to place X-ray collecting optics in front of the target rather than behind to use the higher level of backward-emitted radiation.

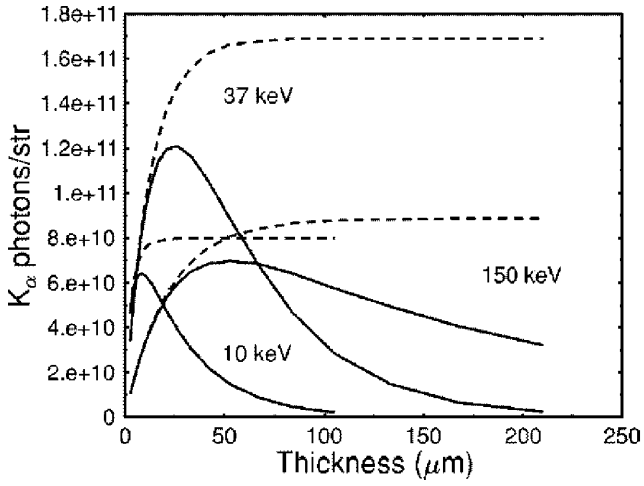

Fig. 4-9: Dependence of forward(solid lines) and backward (dashed lines) K_α emission on target thickness for a Ti foil bombarded by hot electrons with three different temperatures [SRU02].

With the spatially resolved simulations of Salzmann et al.[SRU02], some other statements of Reich et al.[RGU00]have to be modified. The factor between K-shell ionization energy and optimum hot-electron temperature turned out to be *Z*–dependent. For the estimation of optimum gallium parameters, this has little influence: On the one hand the new factor of about 6 is close to the factor of 6.4 (conclusion of /4-4/). On the other hand in non of these simulations elastic scattering is included. This might cause another increase of the optimum electron energy.

The over-all conversion efficiency from laser energy to K_α line radiation has been calculated by Salzmann et al. [SRU02] and is compared to experimental values from different groups using different lasers and targets. The efficiencies from simulations are about 10^{-4} and slightly

decreasing for $Z > 40$. The numbers from the experiments are typically one or two orders of magnitude less between 10^{-5} and 10^{-6}. Taking the numbers from the kHz experiments shown in Table 4-2, one recognizes that for low-energy lasers the efficiency is in the order of about 10^{-7}.

Although the simulations referenced above are calculated for a planar geometry, they should be valid for the cylindrical (jet) geometry without severe restrictions because the geometrical differences are small for emission characteristics precisely in line with the laser or opposite. The differences appear in the spatial effects outside the line of the laser beam. To estimate the particular spatial emission profile from the cylindrical jet target, another simulation (Fig. 4-10) was done by C.W. Siders [CWS01] using the ITS 3.0 simulation package. ITS is a package of different programs using Monte Carlo electron/photon transport codes for 1D (TIGER) as well as 3D (ACCEPT) calculation. All bremsstrahlung cross-sections from 1 keV up to 1 GeV are included. The program keeps track of electron-impact and photo ionization, annihilation radiation etc. Places with extensive information on the package are referenced in the appendix [ITS]. 30 keV hot electrons impinging in a 10 µm focus on a 30 µm gallium jet have been assumed for the simulation. The graph (Fig. 4-10) shows the calculated emission characteristics in a horizontal plane where the laser comes from the left side and the jet target is orthogonal to the paper plane. In the result one recognizes some similarities with the previous simulations, such as the double amplitude for radiation emitted in backward-

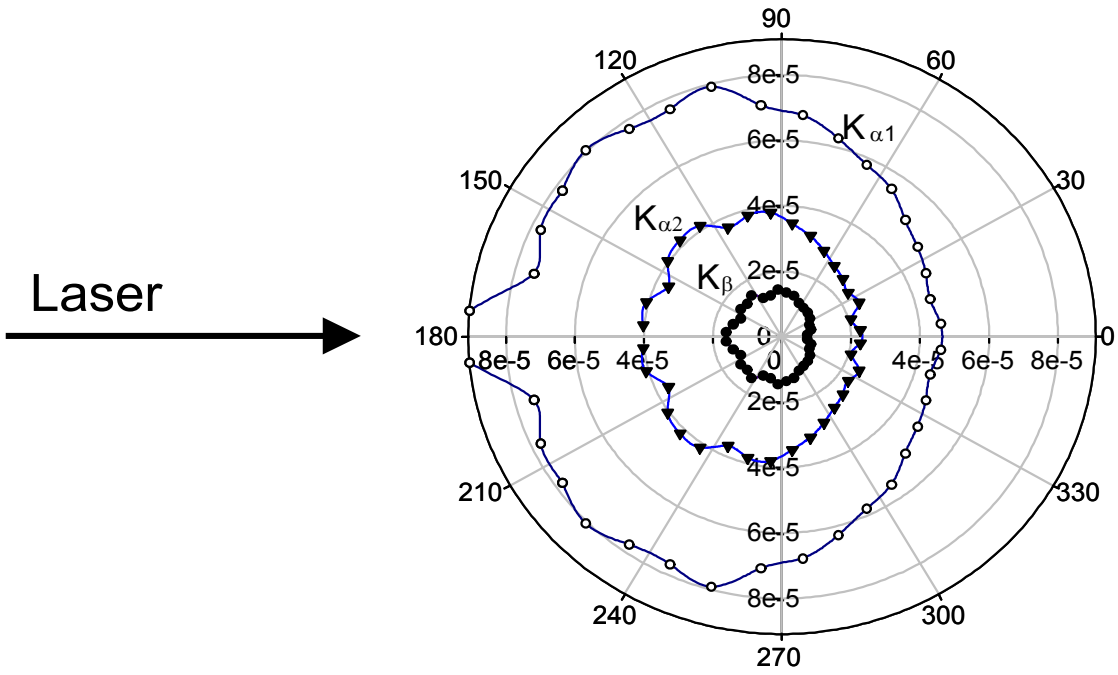

Fig. 4-10: Simulation of X-ray line emission. A 30 µm Ga jet target is bombarded with 30 keV electrons, impinging from the left (after acceleration by the respective laser beam). The target jet is oriented perpendicular to the paper plane [CWS01].

direction (180°, opposite to the laser beam) compared to the radiation emitted into forward direction (0° or inline with laser). The emission perpendicular to jet and laser beam at 90° and 270° is approximately the average of forward and backward emission. A similar simulation for the vertical plane as defined by laser and jet target resulted in an emission intensity decaying to zero for angles close to the jet axis. This is reasonable because in that case the path of the X-ray photons in the material is much longer and hence, reabsorption is more probable.

Finally, a remark should be made concerning X-ray pulse length. For advanced X-ray diffraction experiments this will be a crucial feature. Usually it is assumed that the emission of line radiation starts shortly after the onset of the ultrashort laser pulse. The emission of hard X-rays will continue until the last hot electron is stopped or has left the target.[1] Apparently the scattering processes in a bulk target will cause longer pulses because of longer trajectories inside the material. Calculations have been done [RGU00] to investigate the optimum thickness of target foils for the creation of 100 fs X-ray bursts (90% emission included). The results of 1…3 μm thickness for different target materials seem to be far from experimental reality. Wire targets usually work with diameter ≥ 200 μm and tape targets are not thinner. However, jet targets as presented in this work are one order of magnitude thinner and should therefore offer essentially shorter X-ray pulses. All gallium experiments presented here are done with a diameter of 30 μm, test with thinner jets have shown an enormous increase of jet starting difficulties.

4.2.5 Some Technical Aspects of Gallium X-ray Generation

The generation of X-rays from laser produced plasmas is always connected with the need of high precision in the experimental setup. The most crucial point there is the focus position on the target. In the case of wire, tape or drum targets, extensive control is necessary to prevent or compensate target oscillations and to stabilize its position on a micrometer scale. As shown in the present work (Fig. 3-13 and text thereafter) the laminar jet is inherently stable. Only the nozzle apparatus as a whole needs to be isolated from external vibrations (e.g. pump). In the experiments a certain tendency for drift on a temporal scale of some 10 s was observed. But this can easily be overcome with a closed loop control of the lateral jet position using the power-meter transmission signal as described in the experimental setup (Fig. 4-5 and section 4.2.1). Fig. 4-11 shows the X-ray signal (stars) from the 1 kHz gallium X-ray experiment over

[1] The “afterglow” of the thermal plasma in the soft X-ray region usually remains longer as a low-energy background.

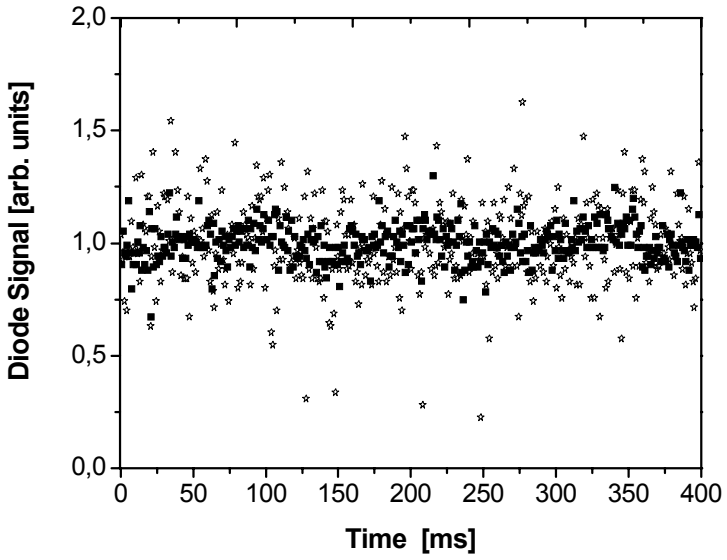

Fig. 4-11: Peak-to-peak stability of gallium X-ray signal (stars denote X-rays, squares the laser). 75% of the X-ray peaks are within ±20% of the average X-ray signal.

a time of 400 ms corresponding to 400 pulses. It is taken using the AXUV –100 silicon diode (International Radiation detectors Inc.) as described in section 4.2.1. Each data point represents the spectrally integrated intensity of the X-ray signal (E > 2 keV) emitted perpendicular to jet and laser. Simultaneously the laser signal (denoted by squares) has been recorded using a DET210 Si diode from Thorlabs, Inc. The standard deviation of the X-ray signal is about 21% and that of the laser is 8%, respectively. Only a few scientific publications mention the source stability. Therefore comparison is difficult. Another jet source using water as soft X-ray source shows a better peak-to-peak stability ([VOG01] found 10% for 250 kHz repetition rate) while in a Cu target experiment by Guo et al. [GUO97] 30 % shot-to-shot fluctuation of the K_α line radiation was detected. For diffraction experiments where the signals are collected and added up over several 100 seconds, the stability as shown here should be fully sufficient. In such cases the long-term stability as shown in Fig. 4-12 is more important.

To investigate the long-term stability during a full experimental session (defined by the jet reservoir) of more than one hour, the radiation was detected with the AMPTEK dispersive silicon spectrometer for about 200 s each 5 min. It should be mentioned that while the jet was running all the time the vacuum chamber was opened between the spectral measurements and evacuated again thereafter. Focusing optics were not changed nor cleaned during the experiment. The remaining changes in the signal (Fig. 4-12) can be due to insufficient

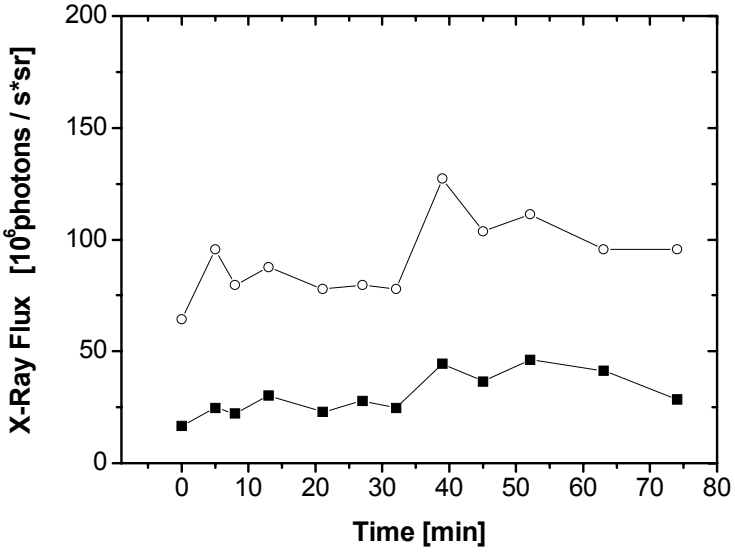

Fig. 4-12: Long term stability of gallium line radiation (full squares for K_α line radiation and open circles for total detected radiation 2 keV<*E*<16 keV).

alignment precision. As mentioned above this can be overcome with an automatic alignment circuit and with higher precision in the alignment stages. The most interesting conclusion of this experiment is the low influence of debris. Debris is a term for the fragments of the target which are expelled during plasma generation. Debris can be ions, atoms, clusters or droplets. Debris can coat optics or destroy (larger particles) sensitive surfaces. Therefore it is a serious problem of all solid-state targets. Gas-jet targets (e.g. [BRH98]) claim to have very low debris. Because of the minimal volume of evaporated target material, liquid-jet targets should exhibit substantially smaller debris production than solid targets. This can only be changed by acoustic waves in the target emanating from the plasma which might destroy larger parts of the jet or even the nozzle. Such effects have not been observed. Nevertheless the debris production of the gallium target is not negligible, e.g., there are ions from the plasma emitted backward. The focusing optics can be sufficiently protected by a pair of strong permanent magnets beside the laser beam. With this protection the transmission of the focusing lens dropped less than 3 % within 1 h of plasma experiments. In forward and side direction more uncharged material is emitted. In these directions all sensitive subjects can be protected by thin plastic foil (e.g. spectrometer, diodes). This was particularly important for the diffraction experiments with the GaAs crystal (section 5.2). There the crystal was protected by lead plates inside the chamber with a small aperture for X-ray transmission and a thin plastic foil which had to be replaced after each experiment.

4.3 Generation of Continuous Radiation (Bremsstrahlung)

In the X-ray spectra of laser produced plasma usually two broadband components are superimposed:

(1) There is the low energy (maximum at less than 1 keV) thermal or black body radiation from the pre-plasma created by a pre-pulse. Its amplitude and its temperature are strongly dependent on the laser contrast; the higher the contrast of the laser pulse the smaller the pre-plasma and the lower the total energy of its emission. In the X-ray spectra presented here the thermal continuum is almost invisible because of absorption in the 25µm Be protection window (Fig. 4-1) and the 10µm Al filter (Fig. 4-5). Only in Fig. 4-16 a) one recognizes the onset of the thermal continuum on the low energy end of the spectrum.

(2) A second broadband component originates from "hot" electrons which are accelerated by the main laser pulse to energies much higher than the plasma temperature. Therefore the bremsstrahlung originating from these electrons is much harder than the emission of the thermal plasma. The center frequency $\nu=E/h$ of the bremsstrahlung component is essentially determined by the kinetic energy of the hot electrons, which in turn depends on the laser intensity (see section 4.2.4).

4.3.1 Estimation of the Hot-Electron Energy

The process for the generation of the high energy broadband component is comparable to the stopping of the electrons in the anode of an X-ray tube (ref. Chapter 2, also mentioned in reviews like [VDL01]). In both cases electrons with an energy of several 10 keV are decelerated in target material behind the critical surface and emit bremsstrahlung. Although the energy distribution of the hot electrons might be different in an LPP and in an X-ray tube, energy conservation is valid for both systems: the emitted photons cannot have more energy than the impinging electrons. Therefore in the spectrum of an X-ray tube (Fig. 4-13-a) the maximum emission frequency ν_{max} is defined by the electron energy $\nu_{max} = e*U/h$ (e is the electron charge, U is the accelerating voltage, h is Planck's constant). For a first order estimate of the energy of the hot electrons, this rule can be applied to the high-energy broadband spectra generated from LPP (Fig. 4-13-b, for details see section 4.3.3). There, the decay of the high-energy broadband spectrum goes down to zero at an energy E_{max} equivalent to the maximum emission frequency ν_{max} in the X-ray tube spectrum. To avoid the ambiguities of high energetic noise or a slow decay, one can extrapolate the decaying high-energy branch of the LPP spectrum by a line and define the intersection with the X-axis as E_{max}.

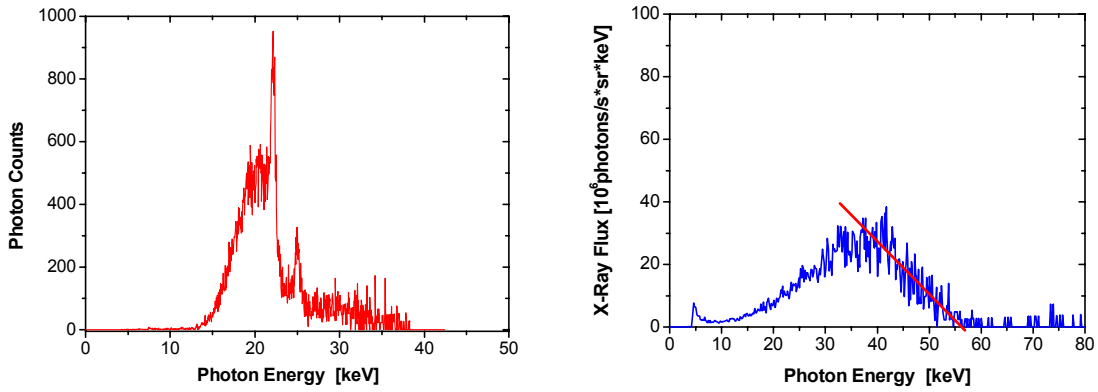

Fig. 4-13 : Bremsstrahlung spectra of a) an X-ray tube with Ag cathode and $E = Ue = 40$ keV [STI02], and b) laser produced plasma from a water target (laser 3×10^{16} W/cm²) with estimated hot electron kinetic energy of $E_{max} = 56$ keV (present work, see Fig. 4-16).

4.3.2 Discussion of Absorption and Re-Absorption Processes

To obtain an estimate for the limitation of bremsstrahlung generation, one can use a similar 2-step approach as in the discussion of the line-radiation emission (section 4.2.4). The absorption of laser energy and conversion into hot electrons depends on the temporal structure of the laser pulse and its contrast as mentioned above. The next step, the conversion of the kinetic energy of the hot electrons into X-ray photons strongly depends on the target material. In this context it is instructive to look at the electron stopping range in different materials to learn more about that. Fig. 4-14 shows the electron stopping range for water, gallium and gold

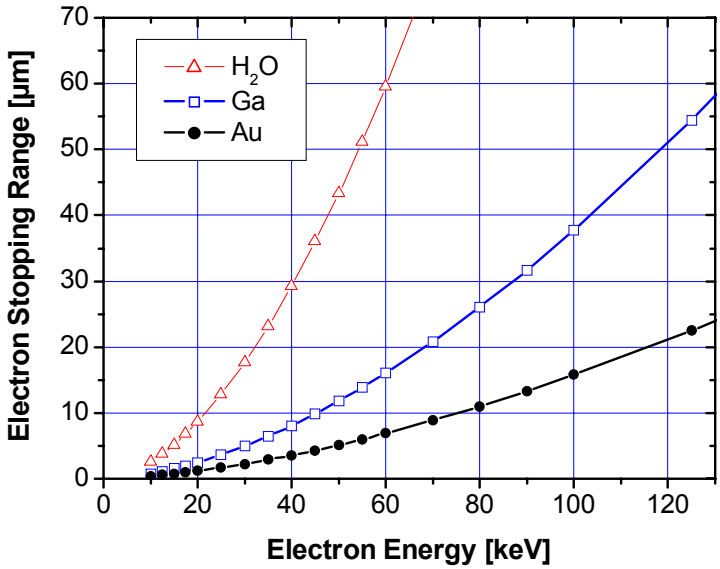

Fig. 4-14: Electron stopping ranges in water (triangles), gallium (squares) and gold (circles) targets.

calculated using the ESTAR[1] online facilities of NIST [NIST02]. In this graph one recognizes several differences for low-Z and high-Z targets. At first it is apparent that not all electrons will be stopped in a 20 or 30 µm water jet target (dominated by Z=8 from oxygen). Especially high-energy electrons will not be absorbed in a thin water target. This leads to a smaller conversion efficiency and to interesting electron effects behind the target which will be discussed in Chapter 6. For high-Z targets (Au: Z=79) or medium-Z (Ga: Z=31) the situation is different. Almost all electrons will be stopped in a thin layer and a 100% conversion of hot electrons into radiation is guaranteed. This also explains the different level of ionizing radiation[2] measured outside the chamber using the precision dose rate meter TOL/F (Berthold Technologies [TOL]): the radiation is probably bremsstrahlung of hot electrons stopped in the chamber walls, which are particularly prominent outside the target if water is used.

For the question of reabsorption of X-ray photons in the target material one can use a comparable estimation and look at the photon attenuation length calculated using the online facilities of LBNL [LBL2]. The results of such a simulation are shown in Fig. 4-15. Again there are large differences for low-Z and high-Z materials. While X-ray photons generated in water will not be stopped in a thin water target (< 50µm) the photons with E<25 keV will hardly traverse more than 10 µm of gold. For gallium the photon attenuation length is longer than the electron stopping range and hence, a large fraction of photons should be able to leave

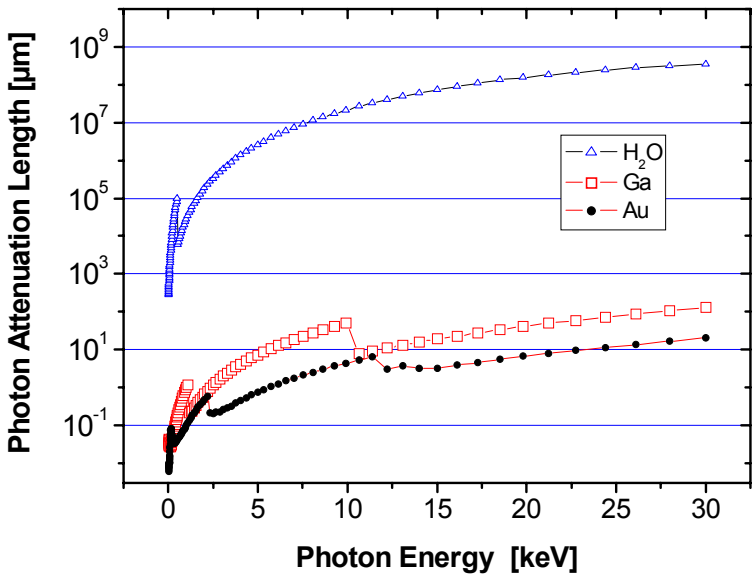

Fig. 4-15: Attenuation length for X-ray photons in different targets (water: triangles, gallium: squares and gold: circles).

[1] With a default option, ESTAR generates stopping powers and ranges for electrons for 72 materials at a standard grid of 81 kinetic energies between 10 keV and 1000 MeV.

[2] Doserate was about 10µSv/h in Ga experiments and up to several mSv/h in water experiments. Therefore in water experiments the doserate may be a valuable help for alignment.

the target. For more detailed information it is necessary to make simulations that include information about the particular target geometry. This would also give more information about the spatial distribution where one would expect a shift from backward to more forward directed photons with increasing photon energy according to the above estimations.

4.3.3 Continuous Spectra from Different Targets

After considering the generation processes, some measured broadband spectra from different targets will be discussed (results shown in Fig. 4-16). It is a comparison of two liquid (gallium and water) and one solid target (gold). The gold (Z=79) target is not only interesting as a high Z-target but also as a close relative of mercury (Z=80) which is a candidate for high-energy X-ray generation using liquid jet targets. The setup of the gold target (drum) is described in the thesis work of U. Vogt [VOG02]. The laser intensity applied was similar for gallium and water target (3×10^{16}W/cm²) while for the gold experiments a different laser system with two energy settings has been used (1 kHz, 25 fs, first curve: 350μJ, 2×10^{16} W/cm² , 2nd curve 500μJ, 3×10^{16} W/cm²). The setup was the same as in the line-radiation experiments with one exceptions: For the gold spectra the spectrometer was covered with a 12 μm aluminum filter.
Both the water and the gallium spectrum show an increase towards low energies which can be attributed to the emission of low-energy thermal radiation from the pre-plasma. A comparison with the efficiency curve Fig. 4-1 indicates that this increase is much larger than in the not re-calibrated low energy end of the spectra in Fig. 4-16. The center of the spectra is located at about 37 keV, similarly for gallium and water. The estimated kinetic energy of the hot electrons is about 55 keV, also for both target materials, gallium and water. This is about one third less than the 88 keV estimated from the laser intensity of 3×10^{16} W/cm² in equation 4-2. The difference demonstrates that the conversion efficiency of laser intensity into electron energy may still be improved (see section 4.2.3).
The similar hot-electron temperatures of the spectra in Fig. 4-16 a) and b) emphasize that the energy transfer from the laser pulse to the hot electrons is almost independent of the target material. In contrast to this the amplitude in the gallium curve is about three times higher than in the water spectrum. This indicates a different conversion efficiency from electron energy into bremsstrahlung depending on the Z of the target material and may be explained by the different absorption cross-sections (see also Fig. 4-14). These results are shown here for the observation angle of 90 degrees. For a general comparison of the conversion efficiency, one has to take the spatial distribution into account. Finally, it is interesting to note that the flux of the broadband radiation of gallium is comparable to the line-radiation flux.

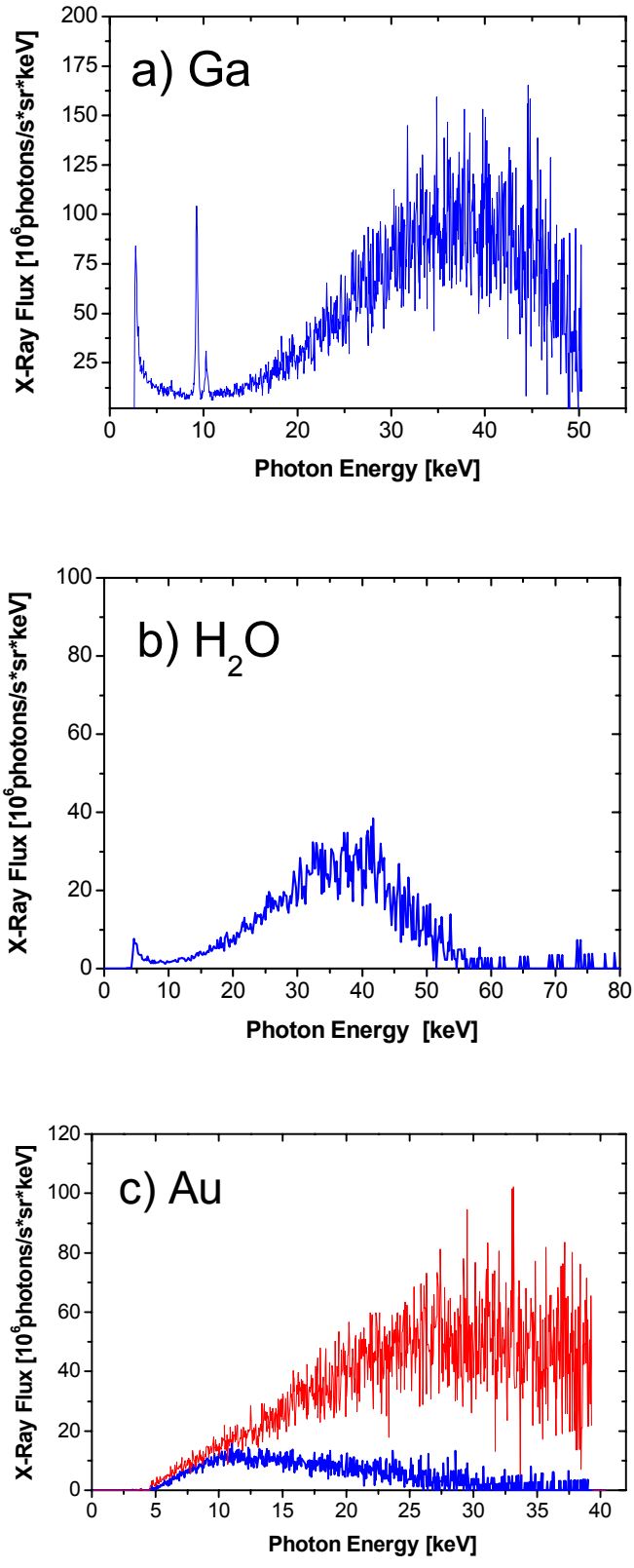

Fig. 4-16: Broadband X-ray spectra from different targets: a) gallium at a laser intensity I=3×10^{16}W/cm² , 50fs pulse length, b) water (I=3×10^{16}W/cm², 50 fs), c) gold (blue: I=2×10^{16}W/cm², red: 3×10^{16}W/cm², 25 fs).

In the case of the gold target the change of the emission spectra with increasing laser intensity is apparent (Fig. 4-16 c). It is not only a simple shift of the distribution but an increase of amplitude too, so that the lower energy spectrum appears within the envelope of the higher energy spectrum. This behavior can be expected for other target materials as well and gives a general idea of the laser-intensity dependent tunability of this broadband radiation source. The amplitude of the gold curve is on the same order of magnitude as in the other spectra but somewhat lower than in the case of gallium. It can be concluded that a mercury target would not offer remarkable advantages in efficiency compared to a gallium target. This is important and represents a second reason to discard mercury as a target material beside the poisonous character of the material.

Finally, some future prospects for the generation of broadband X-ray radiation with liquid targets are discussed. Although the characteristics of the broadband radiation would have to be investigated in more detail (e.g. stability), the fact that the magnitude of the gallium spectrum is comparable to the line radiation opens up interesting possibilities for experimental use. With the application of a monochromator, a tunable source of hard X-rays appears feasible. Focusing of the radiation with a bent crystal could increase the intensity available for experiments. The advantages such as small source size (on the order of 10 μm), sub-ps pulse duration and 1 kHz repetition rate should be similar to those of the line-radiation source discussed earlier. The water jet appears in this respect even more attractive because the experimental handling is much easier. Running time can be easily extended to many hours by using larger tanks, still the target costs are almost nothing. The lower emission magnitude might be improved by using a jet with larger diameter. However, one disadvantage of water is a much higher vapor pressure in comparison to gallium, for high vacuum applications this might cause problems. But because of the good transmission of hard X-rays through several materials this could be overcome with a target chamber separated from the actual experiment by a thin window (e.g. Al). This would completely solve the debris problem too. Hence, for future experiments with monochromatic X-ray line-radiation the Ga-jet target is to be favoured, while for the generation of broadband hard X-rays in the range of 20…50 keV a setup based on a water jet of 30 μm diameter (or more) in a separated target chamber would be the an interesting alternative.